Quantum Theory of Electronic Excitation and Sputtering by Transmission Electron Microscopy

Anthony Yoshimura[1,2*], Michael Lamparski[2], Joel Giedt[2],
David Lingerfelt[3], Jacek Jakowski[3], Panchapakesan Ganesh[3], Tao Yu[4],
Bobby Sumpter[3], and Vincent Meunier[2,5]

[1] *Lawrence Livermore National Laboratory, Livermore, CA 94550, USA*
[2] *Department of Physics, Applied Physics, and Astronomy, Rensselaer Polytechnic Institute, Troy, New York 12180, USA*
[3] *Center for Nanophase Material Sciences, Oak Ridge National Laboratory, Oak Ridge, TN 37831, USA*
[4] *Department of Chemistry, University of North Dakota, Grand Forks, ND 58202, USA*
[5] *Department of Materials Science and Engineering, Rensselaer Polytechnic Institute, Troy, NY 12180, USA*
[*] *Correspondence to be addressed to yoshimura4@llnl.gov*

S1   Invariant matrix element $\mathcal{M}$

As the excitation amplitude in equation (16) contains the invariant matrix element $\mathcal{M}$ and not $|\mathcal{M}|^2$, we are unable to use the spin sum identities typically used to derive many QED cross sections.[1,2] Nonetheless, the evaluation of $\mathcal{M}$ in equation (4) is straightforward, though a bit cumbersome. In the Dirac basis,[3]

$$\gamma^0 = \begin{pmatrix} I & 0 \\ 0 & -I \end{pmatrix} \quad \text{and} \quad \gamma^i = \begin{pmatrix} 0 & \sigma^i \\ -\sigma^i & 0 \end{pmatrix}, \tag{S1}$$

where

$$I = \begin{pmatrix} 1 & 0 \\ 0 & 1 \end{pmatrix} \quad \text{and} \quad \vec{\sigma} = \left\{ \begin{pmatrix} 0 & 1 \\ 1 & 0 \end{pmatrix}, \begin{pmatrix} 0 & -i \\ i & 0 \end{pmatrix}, \begin{pmatrix} 1 & 0 \\ 0 & -1 \end{pmatrix} \right\}. \tag{S2}$$

The electron spinors in equation (4) can be written as

$$u^1(p) = \sqrt{\epsilon + m} \begin{pmatrix} 1 \\ 0 \\ \dfrac{p^z}{\epsilon + m} \\ \dfrac{p^x + ip^y}{\epsilon + m} \end{pmatrix} \quad \text{and} \quad u^2(p) = \sqrt{\epsilon + m} \begin{pmatrix} 0 \\ 1 \\ \dfrac{p^x - ip^y}{\epsilon + m} \\ \dfrac{-p^z}{\epsilon + m} \end{pmatrix}, \tag{S3}$$

while

$$\bar{u}^s(p) = u^{s\dagger}(p)\gamma^0. \tag{S4}$$

As justified in the subsection titled *Scattering of free electrons*, we need only evaluate the t-channel contribution to $\mathcal{M}$ and multiply the result by 2. That is,

$$\mathcal{M}(p_4 p_3 \leftarrow p_2 p_1) \sim e^2 \sum_{s_1,s_2,s_3,s_4} \bar{u}^{s_4}(p_4)\gamma^\mu u^{s_1}(p_1) \left(\frac{1}{p_3 - p_2}\right)^2 \bar{u}^{s_3}(p_3)\gamma_\mu u^{s_2}(p_2). \tag{S5}$$

Substituting equations (S1) through (S4) into (S5) yields $\mathcal{M}$ in terms of the components of the electrons' 4-momenta. That is,

$$\begin{aligned}
\mathcal{M}(p_4 p_3 \leftarrow p_2 p_1) \sim -\frac{2e^2}{(p_3 - p_2)^2} & \left[(\epsilon_1 + m)(\epsilon_2 + m)(\epsilon_3 + m)(\epsilon_4 + m)\right]^{-1/2} \\
\times \Big\{ & (\epsilon_1 + m)p_4^x \left[(\epsilon_2 + m)p_3^x + (\epsilon_3 + m)p_2^x\right] \\
& + 2(\epsilon_1 + m)(\epsilon_3 + m)(p_2^y + ip_2^z)(p_4^y - ip_4^z) \\
& + 2(\epsilon_2 + m)(\epsilon_4 + m)ip_1^z(p_3^y - ip_3^z) \\
& - \left[(\epsilon_2 + m)(\epsilon_3 + m) + p_2^x p_3^x + (p_2^y + ip_2^z)(p_3^y - ip_3^z)\right] \\
& \quad \times \left[(\epsilon_1 + m)(\epsilon_4 + m) + ip_1^z(p_4^y - ip_4^z)\right] \Big\},
\end{aligned} \tag{S6}$$

where we let p_1 denote the momentum of the beam electron so that $p_1^x = p_1^y = 0$. See the Mathematica[4] notebook in the Supporting Information for more details.

S2   Normalization

When integrating over 4-momentum space as is done in the subsection titled , Lorentz invariance constrains a particle's 4-momentum to obey $p^2 = m^2$. It follows that the 4-momentum integration measure d^4p is always multiplied by a delta function $\delta(p^2 - m^2)$, *i.e.*,

$$d^4p\, \delta(p^2 - m^2)\theta(p^0) = \frac{d^4p}{2p^0}\delta(p_0 - \epsilon_{\mathbf{p}}), \tag{S7}$$

where the Heaviside step function restricts our consideration to particles of positive mass (we note that antiparticles are interpreted as positive mass particles that propagate backwards in time). With this integration measure, the identity operator can be written as

$$\begin{aligned}
\hat{I} &= \int \frac{d^4p}{(2\pi)^4}(2\pi)\delta(p^2 - m^2)\theta(p^0)\,|p\rangle\,\langle p| \\
&= \int \frac{d^3p}{(2\pi)^3 2\epsilon_{\mathbf{p}}}\,|p\rangle\,\langle p| \\
&= \int \frac{d^3p}{(2\pi)^3}\,|\mathbf{p}\rangle\,\langle\mathbf{p}|\,.
\end{aligned} \tag{S8}$$

The last equality implies that

$$|p\rangle = (2\epsilon_{\mathbf{p}})^{1/2}\,|\mathbf{p}\rangle\,. \tag{S9}$$

S3   Lab frame p_3^z

For the scattering of two free electrons, conservation of 4-momentum allows us to write

$$p_1 + p_2 = p_3 + p_4. \tag{S10}$$

This constrains four of the six components needed to specify the 3-momenta of the two outgoing particles, so that only two componenets are independent. We choose the independent components to be p_3^x and p_3^y. Thus, we wish to find p_3^z as a function of p_1, p_2, p_3^x, and p_3^y. From this, $p_4 = p_1 + p_2 - p_3$ is easily obtained, and we have all six components of outgoing 3-momenta needed to calculate the scattering amplitude from equation (16). We start by setting the z-direction parallel to $\mathbf{p}_1$. This means that

$$
\begin{aligned}
p_4^x &= p_2^x - p_3^x \\
p_4^y &= p_2^y - p_3^y \\
p_4^z &= p_1^z + p_2^z - p_3^z \\
\epsilon_4 &= \epsilon_1 + \Delta\epsilon
\end{aligned}
\tag{S11}
$$

where

$$\epsilon_i = \epsilon_{\mathbf{p}_i} = \sqrt{\mathbf{p}_i^2 + m^2}, \qquad \Delta\epsilon = \epsilon_{n\mathbf{k}} - \epsilon_{n'\mathbf{k}'}, \tag{S12}$$

and $\epsilon_{n\mathbf{k}}$ and $\epsilon_{n'\mathbf{k}'}$ are the eigenvalues of the excited hole and electron states, respectively. We can also write $\epsilon_1 = \gamma m$ where $\gamma = 1/\sqrt{1 - \beta^2}$ is the Lorentz factor corresponding to the beam electron's velocity β. Squaring the last line in (S11) and subtracting m^2 then gives

$$\mathbf{p}_4^2 = \mathbf{p}_1^2 + 2\gamma m \Delta\epsilon + \mathcal{O}(\Delta\epsilon^2). \tag{S13}$$

We can ignore terms of order $\mathcal{O}(\Delta\epsilon^2)$ since $\Delta\epsilon \ll m$. Meanwhile, squaring and summing the first three equations in (S11) tells us that

$$\mathbf{p}_4^2 = \mathbf{p}_1^2 + \mathbf{p}_2^2 + \mathbf{p}_3^2 + 2\left[p_1^z p_2^z - \mathbf{p}_2^\perp \cdot \mathbf{p}_3^\perp - (p_1^z + p_2^z)p_3^z\right], \tag{S14}$$

where the $\perp$ superscript denotes the projection perpendicular to $\hat{z}$. Subtracting equation (S14) from equation (S13) then yields

$$0 \sim \mathbf{p}_2^2 + \mathbf{p}_3^2 + 2\left[p_1^z p_2^z - \mathbf{p}_2^\perp \cdot \mathbf{p}_3^\perp - (p_1^z + p_2^z)p_3^z\right] - 2\gamma m \Delta\epsilon. \tag{S15}$$

Asymptotic formula (S15) can then be solved for p_z^3, so that

$$p_3^z \sim p_1^z + p_2^z \pm \sqrt{\left(p_1^z\right)^2 - \left(\mathbf{p}_2^\perp - \mathbf{p}_3^\perp\right)^2 + 2\gamma m \Delta\epsilon}. \tag{S16}$$

We choose the $-$ from $\pm$ as we impose that $\mathbf{p}_3$ is a component of the outgoing crystal electron state, whose z-momentum is much smaller than that of the beam electron.
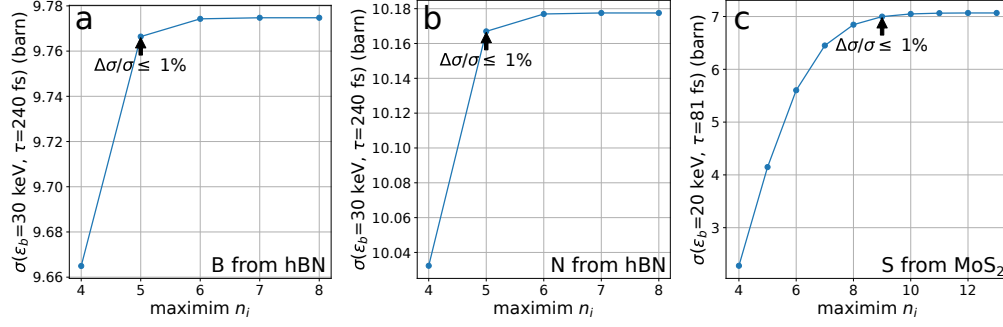
S4   Converging n_i^{max}

Figure S1: Convergence of the sputtering cross section with respect to the maximum number of beam-induced excitations n_i^{max} considered. The simulated beam energies ϵ_b are the lowest experimental beam energies used for each material. The excitation lifetimes τ are those used to fit the experimental data in figures 5 and 6. Each cross section is deemed converged when any increase in n_i^{max} increases the cross section by less than 1%.

S5   Peaks in the sputtering cross section of hBN

Figure S2: The sputtering cross sections of boron and nitrogen from the hBN armchair edge peak at beam energies much lower than those typically used for microscopy and defect engineering. However, as mentioned in the main text, the validity of our perturbative approximation to the scattering operator breaks down at low beam energies (see *Probability of n_i excitations*). Thus, the values and positions of these peaks may change if higher order perturbation terms are considered.
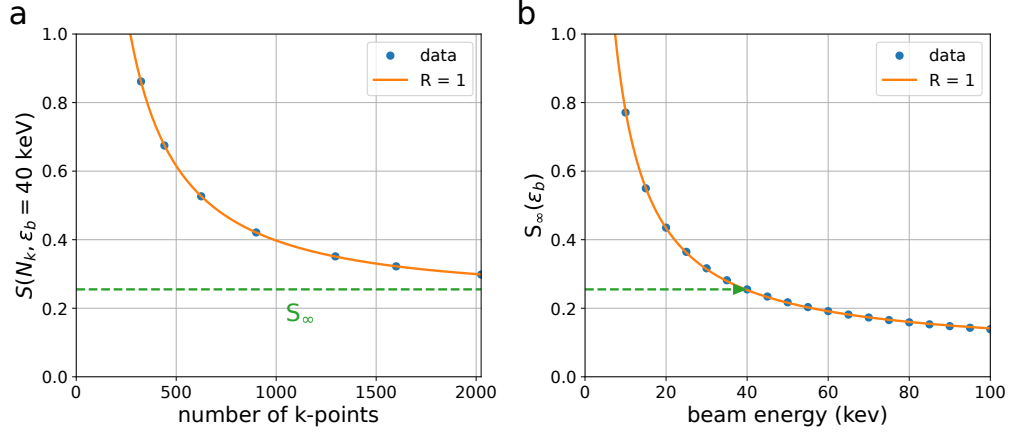
S6   Fitting and converging S

Figure S3: Finding the large crystal limit of $S(\epsilon_b)$ requires extrapolation. Panel (a) shows the dependence of S on the number k-points N_k in the Brillouin zone of hBN under 40 keV irradiation. The simulated points are fitted well by equation (S17). The green dashed line denotes S_∞, the asymptotic limit of $S(N_k)$ for large N_k. Panel (b) then shows the dependence of S_∞ on the beam energy ϵ_b, which is fitted well by equation (S18). The green arrow in panel (b) illustrates how $S_\infty(\epsilon_b = 40$ keV$)$ is determined by the fit in panel (a).

For a given beam energy ϵ_b, we calculate the sum of all transition probabilities S defined in equation (18) for various k-point densities where the number of k-points in the Brillouin zone is N_k. We then fit the points to a curve of the form

$$S(N_k, \epsilon_b) = \frac{a}{N_k - b} e^{-cN_k} + S_\infty, \qquad (S17)$$

where a, b, c, and S_∞ are all fitting parameters that depend on ϵ_b (figure S3a). We repeat this for multiple values of ϵ_b ranging from 5 to 100 keV and record the best fit S_∞ for each ϵ_b. Based on the work of Bethe,[5,6,7] we fit the resulting values of $S_\infty(\epsilon_b)$ to an inverse function,

$$S_\infty(\epsilon_b) = \frac{A}{\epsilon_b - B} + C. \qquad (S18)$$

where A, B, and C are fitting parameters. The parameters for hBN and MoS_2 are given in table S1. The fitted curve can then be substituted for $S(\epsilon_b)$ in formula (23) to obtain $P_i(\epsilon_b, n_i)$, the probability of exciting n_i electrons in the large crystal limit.

Finally, S must also be converged with respect all parameters. These include the maximum virtual photon momentum, DFT cutoff energy, and height of the pristine unit cell (figure S4). S is considered converged with respect to a parameter when any increase in the parameter's precision changes S by less than 5%.

material	A (eV)	B (eV)	C
hBN	7.655	-0.770	0.06526
MoS$_2$	49.05	-3.867	0.3547

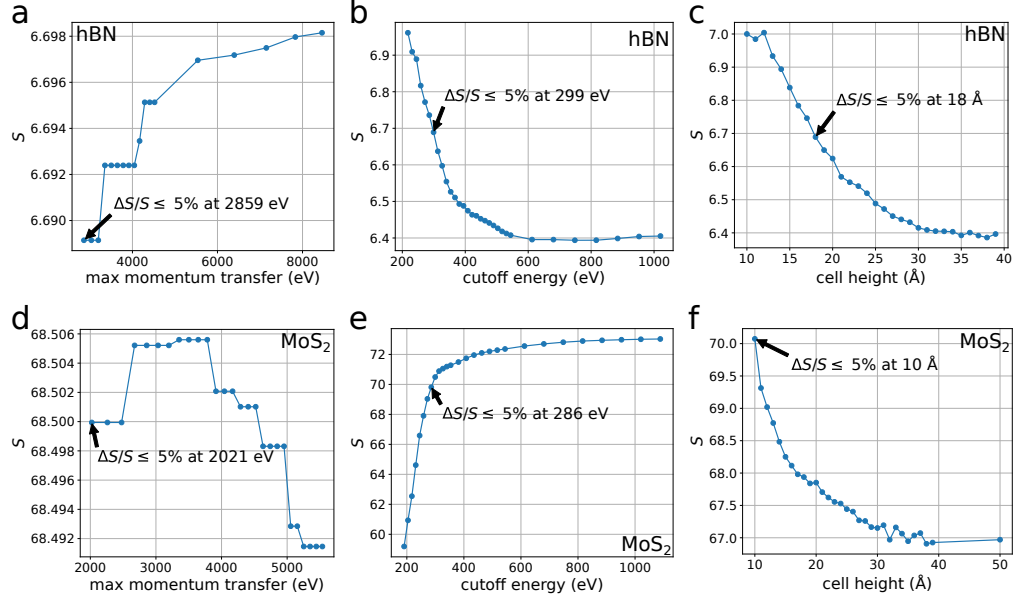Table S1: Fitting parameters of equation (S18) for hBN and MoS$_2$.

Figure S4: Convergence of S with respect to the (a and d) maximum magnitude of virtual photon momentum considered, (b and e) plane-wave DFT cutoff energy, and (c and f) height of the unit cell. A $6 \times 6 \times 1$ k-point mesh and a beam energy of 60 keV is used to generate all six plots. The converged parameters were found to be insensitive to changes in k-point density and beam energy. S is deemed converged when any increase in precision changes S by less than 5%.
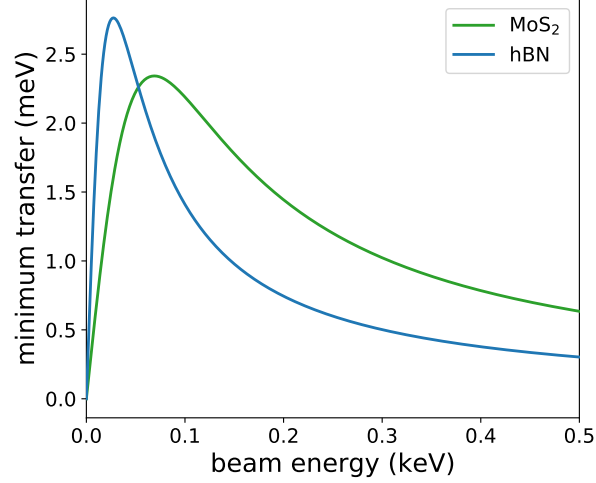
S7 Calculating E_{min}

Figure S5: The minimum energy transfer from the beam electron to the target nucleus peaks at very low beam energies and is always much smaller than the nuclei's average thermal kinetic energy of $\sim$39 meV at room temperature.

In hBN, a unit cell contains a boron and nitrogen atom. As these atoms have similar masses and displacement thresholds (table 1), the sputtering of both atoms should be considered for a given beam energy. Thus, we approximate the maximum cross sectional area σ_{max} of these atoms to be $\Omega_{\mathrm{hBN}}/2$, where Ω_{hBN} is the area of the hBN unit cell. On the other hand, molybdenum is much heavier than sulfur and has a much larger displacement threshold in $\mathrm{MoS_2}$.[8] This means that only the sputtering of sulfur needs to be considered. Additionally, of the two sulfur atoms in the $\mathrm{MoS_2}$ unit cell, only the atom on the outgoing surface is eligible to sputter from a pristine system.[8] Therefore, σ_{max} for sulfur sputtering from $\mathrm{MoS_2}$ is $\Omega_{\mathrm{MoS_2}}$, the area of the $\mathrm{MoS_2}$ unit cell.

To approximate E_{min}, we use the Rutherford displacement cross section[9,10,11] as an approximation to equation (2),

$$\sigma_R = \pi \left(\frac{Z\alpha}{|\mathbf{p}|\beta} \right)^2 \left(\frac{E_{\mathrm{max}}}{E_d} - 1 \right). \tag{S19}$$

Setting $\sigma_R = \sigma_{\mathrm{max}}$ and $E_d = E_{\mathrm{min}}$ and solving for E_{min} yields

$$E_{\mathrm{min}}(\epsilon_b) = E_{\mathrm{max}} \left[\frac{\Omega}{\pi} \left(\frac{|\mathbf{p}_b|\beta}{Z\alpha} \right)^2 + 1 \right]^{-1}. \tag{S20}$$

Using the Rutherford cross section instead of the McKinley-Feshbach cross section should be accurate for small beam energies for which $\beta \ll 1$. This makes it well-suited for finding E_{min}, since $E_d(n_f) < E_{\mathrm{min}}$ only for large n_f, and large n_i (and thus n_f) are much more likely for small beam energies (figure 3).

9

With that said, the sputtering cross section is fairly insensitive to the exact value of $E_{\min}$ when $E_{\min} \ll E_{\max}$. This is because the post-collision velocity of the PKA diminishes when the energy transfer E shrinks. The beam-induced excitations therefore have more time to relax before the PKA reaches the step in the energy surface (see *Effect of excitations on the displacement threshold*). This makes P_f small for small E, so that contributions to the integral in equation (3) are extremely tiny for E near $E_{\min}$. As a result, changes in $E_{\min}$ are essentially immeasurable for beam energies greater than 1 keV. Nonetheless, the use of $E_{\min}$ is necessary for the calculation of a finite sputtering cross section.

References

[1] Peskin, M. E.; Schroeder, D. V. *An Introduction to Quantum Field Theory*, 1st ed.; Perseus Books Publishing, L.L.C.: Reading, MA, 1995.

[2] Lancaster, T.; Blundell, S. J. *Quantum Field Theory for the Gifted Amateur*, 1st ed.; Oxford University Press: New York, NY, United States of America, 2014; p 350.

[3] Bjorken, J. D.; Drell, S. D. *Relativistic Quantum Mechanics*; International series in pure and applied physics; McGraw-Hill, 1964.

[4] Inc., W. R. Mathematica, Version 12.3. `https://www.wolfram.com/mathematica`.

[5] Bethe, H. *Ann. Phys.* **1930**, *397*, 325–400.

[6] Susi, T.; Meyer, J. C.; Kotakoski, J. *Nat. Rev. Phys.* **2019**, *1*, 397–405.

[7] Kretschmer, S.; Lehnert, T.; Kaiser, U.; V. Krasheninnikov, A.; Krasheninnikov, A. V. *Nano Lett.* **2020**, *20*, 2865–2870.

[8] Komsa, H. P.; Kotakoski, J.; Kurasch, S.; Lehtinen, O.; Kaiser, U.; Krasheninnikov, A. V. *Phys. Rev. Lett.* **2012**, *109*, 035503–1–5.

[9] Thornton, S. T.; Marion, J. B. *Classical Dynamics of Particles and Systems*, 5th ed.; Brooks/Cole: Boston, MA, 2004.

[10] Sakurai, J. J.; Napolitano, J. *Modern Quantum Mechanics*, 2nd ed.; Pearson Education: San Fransisco, CA, 2011.

[11] Yoshimura, A.; Lamparski, M.; Kharche, N.; Meunier, V. *Nanoscale* **2018**, *10*, 2388–2397.